PAPER

Check for updates

Two-step vapor deposition of self-catalyzed large-size PbI$_2$ nanobelts for high-performance photodetectors†

Mingming Han,‡[a] Jiamin Sun,‡[ab] Luozhen Bian,‡[ab] Zhou Wang,[c] Lei Zhang,[d] Yanxue Yin,[a] Zhaofeng Gao,[a] Fulin Li,[a] Qian Xin,[a] Longbin He, [iD][d] Ning Han,*[c] Aimin Song[a] and Zai-xing Yang [iD] *[ab]

The grown lead iodide (PbI$_2$) is usually a two-dimensional sheet with a finite size which necessitates sophisticated device metallization and the growth of quasi one-dimensional materials is still challenging. In this work, large-size (length > 100 μm), single-crystalline and high-density PbI$_2$ nanobelts are successfully synthesized by manipulating the microenvironment in a two-step vapor deposition process at a slow heating rate of ∼18 °C min^{-1}. Firstly, PbI$_2$ nanosheet seeds are grown by physical vapor deposition, and then PbI$_2$ nanobelts are synthesized by a self-catalyzed vapor–liquid–solid growth mechanism, which is verified by the Pb nanoparticles on the nanobelt tips. Photoluminescence and ultraviolet-visible spectra show the uniform high-quality crystallinity of the as-prepared large-size PbI$_2$ nanobelts with a bandgap of 2.36 eV. When configured into photodetectors with a shadow mask, the fabricated device exhibits a low dark current of 4 pA, an impressive ON/OFF current ratio of 10^3–10^4, a photoresponsivity of 13 mA W^{-1}, and a fast response with the rise and decay time constants of 425 and 41 ms, respectively. All these performances are comparable to those of state-of-the-art layered PbI$_2$ nanostructure photodetectors, but the ease of synthesizing large-size PbI$_2$ nanobelts may have a useful impact on next-generation easily-fabricated high-performance optoelectronics.

Introduction

In the past decade, layer-structured materials with in-plane covalent bonding and weak interlayer interactions (van der Waals) have attracted extensive research attention, owing to the possibility of thinning down to atomically thick two-dimensional (2D) materials.[1–13] As a typical layered perovskite derivative, lead iodide (PbI$_2$) has attracted extensive research attention in solar cells, photodetectors and other optoelectronic devices,[14–26] due to its direct bandgap of 2.28–2.5 eV and tunable optoelectronic properties.[16,19–27] The layered PbI$_2$ material is composed of covalently bonded I–Pb–I repeating units stacked along the c-axis by van der Waals interlayer interaction.[28,29] Up to now, low dimensional PbI$_2$ nanostructures of nanosheets,[19–22,24,26] nanowires[19,23,27] and atomically thin monolayers[22] have been prepared by a simple synthesis method of vapor deposition. In the reported vapor deposition of PbI$_2$ nanostructures, the one-dimensional (1D) nanowires followed a chemical vapor deposition (CVD) process,[19,23,27] while, the two-dimensional (2D) nanosheets followed a physical vapor deposition (PVD) process.[19,21,22,26] For example, Meyers et al. reported recently the self-catalyzed vapor–liquid–solid (VLS) growth of PbI$_2$ nanowires in a CVD growth procedure.[23] On the other hand, highly uniform 2D PbI$_2$ nanosheets have been prepared by Wang et al. via a space confined PVD process.[26] Furthermore, Lan et al. pointed out that the surface roughness of the growth substrates played a critical role in the nucleation of PbI$_2$ microplanes in the PVD growth of 2D PbI$_2$ nanosheets.[21] However, for photodetector application, 1D nanowires have a relatively smaller absorption area leading to the low current density and 2D nanosheets with a finite size necessitate complicated device metallization such as the Au nanowire mask method.[19,22] Therefore, it is highly desirable to synthesize large-size 2D materials for easily fabricated photodetectors.

[a] Center of Nanoelectronics and School of Microelectronics, Shandong University, Jinan 250100, P. R. China. E-mail: zaixyang@sdu.edu.cn

[b] Shenzhen Research Institute of Shandong University, Shandong University, Shenzhen 518057, P. R. China

[c] State Key Laboratory of Multiphase Complex Systems, Institute of Process Engineering, Chinese Academy of Sciences, Beijing 100190, P. R. China. E-mail: nhan@ipe.ac.cn

[d] SEU-FEI Nano-Pico Center, Key Lab of MEMS of Ministry of Education, Collaborative Innovation Center for Micro/Nano Fabrication, Device and System, Southeast University, Nanjing 210096, P. R. China

† Electronic supplementary information (ESI) available. See DOI: 10.1039/c8tc01180j

‡ These authors contributed equally to this work.

5746 | *J. Mater. Chem. C*, 2018, **6**, 5746–5753

This journal is © The Royal Society of Chemistry 2018

Combining the geometry of 1D nanowires with 2D nanosheets, the quasi 1D nanostructure of the 2D nanobelt is considered as a promising candidate for achieving high performance and easily fabricated optoelectronic devices. Up to now, most of the studies have been concentrated on the 2D morphologies with grain sizes on the order of tens of micrometers,[19,22,24,26] there are limited reports focusing on the large-scale synthesis of 2D PbI_2 nanobelts with sizes of up to hundreds of micrometers in a CVD process. With a size of up to hundreds of micrometers, it will become easier to handle these 2D nanomaterials in real optoelectronic applications. In this work, large-scale PbI_2 nanobelts with lengths of up to hundreds of micrometers (>100 μm) have been prepared successfully on amorphous SiO_2/Si substrates *via* a two-step thermal evaporation process. Firstly, the hexagonal layered PbI_2 nanosheets are formed on the growth substrate when the source material of PbI_2 is at a low thermal temperature, following a PVD growth process. With the increase of the heating temperature, the PbI_2 nanobelts grow from the as-grown PbI_2 nanosheet seed layer by a self-catalyzed CVD process. The mass of the source material, growth temperature and growth time are found to be essential issues in the controllable growth of large-size and high-density PbI_2 nanobelts. Without adopting any sophisticated device fabrication process, the as-prepared large-size PbI_2 nanobelts can be configured into simple photoconductors by a shadow mask, exhibiting impressive photosensing properties with a small dark current of 4 pA, an impressive ON/OFF current ratio of 10^3–10^4, and a good responsivity of 13 mA W^{-1} at a wavelength of 445 nm, excellent stability and an efficient time response (*i.e.*, rise and decay time constants of 425 and 41 ms, respectively). All these results confirm evidently the technological potency of these large-size and highly crystalline 2D PbI_2 nanobelts for easily-fabricated high-performance photodetectors.

Experimental

PbI_2 nanobelts synthesis

The large-size PbI_2 nanobelts studied here were synthesized by employing a solid-source CVD method in a horizontal tube furnace, similar to that of the reported literature.[19,21–23,26,27,30–32] In brief, the solid source of PbI_2 powder (99.99% purity) was located upstream and the growth substrate of SiO_2/Si was located downstream of a two-zone tube furnace with a distance of 5.5 cm. Argon (99.999% purity) was used as the carrier gas to transport the thermally vaporized material downstream. Prior to heating, the quartz tube was purged with 50 standard cubic centimeter (sccm) Ar for 0.5 h. During growth, the source material of PbI_2 was heated to 550 °C in 30 min ($\sim$18 °C min^{-1}) and was kept at this temperature for 20 min. As shown in the temperature distribution of the downstream zone (Fig. S1, ESI†), the growth temperature of the large-size PbI_2 nanobelts is deduced to be $\sim$364 °C. After the growth, the heating of PbI_2 was stopped and it was cooled to room temperature naturally in an Ar flow. Eventually, a layer of orange yellow product could be collected on the substrate.

Material characterization

Surface morphologies of the as-grown large-size PbI_2 nanobelts were examined using a scanning electron microscope (SEM, Nova NanoSEM 450, FEI Company) and a transmission electron microscope (TEM, FEI TECNAI 20). The thickness of the as-prepared large-size PbI_2 nanobelts were measured using an atomic force microscope (AFM, CSPM5500, Being Nano-Instruments). The crystal structure and crystallinity of the products were verified by X-ray diffraction (XRD, D8 Advance, Bruker) and selected area electron diffraction (SAED) coupled with TEM. Elemental identifications were performed using an energy dispersive X-ray spectroscopy (EDS) detector attached to SEM to measure the chemical composition of the obtained nanobelts. For the TEM studies, the nanobelts were scratched onto the copper grid for the corresponding characterization. Raman and photoluminescence (PL) spectra followed by PL and Raman mappings were measured by using a Raman spectrometer (inVia Reflex, Renishaw) with a 532 nm laser and 325 nm laser, respectively. The corresponding absorbance spectrum was measured using a UV-vis spectrometer (TU-1901, Beijing Puxitongyong Company).

Nanobelt device fabrication and photo-electrical property measurements

For the device fabrication, the nanobelts were firstly transferred onto degenerately doped p-type Si substrates with a 300 nm thick thermally grown gate oxide layer by using a physical dry transfer technique. A stainless steel grid was next used as the shadow mask and attached onto the substrate. Ti (5 nm) and Au (200 nm) thin films were deposited *via* electron beam evaporation as the electrical contact electrode. The electrical performance of the fabricated device was then characterized with a standard Lakeshore electrical probe station and a Keithley 4200 semiconductor analyzer. Laser diodes with wavelengths of 375, 445, 532, 630 and 730 nm were used as the light source for the photodetector measurement, while the power of the incident irradiation was tuned and measured using a power meter from 15 to 150 mW cm^{-2}.

Result and discussions

SEM together with EDS technology are adopted here to characterize the morphology and composition of the as-prepared large-size PbI_2 nanobelts. With an optimal growth condition of 0.015 g PbI_2 powder as source material, large-size PbI_2 nanobelts with high density have been prepared successfully on an amorphous substrate at 550 °C for 20 min under a 50 sccm Ar atmosphere. As shown in Fig. 1a, the as-grown sample shows the morphology of nanobelts with a smooth surface and a length of >100 μm. At the same time, the composition of this large-size nanobelt is detected by EDS, showing the nanobelt body consists of Pb and I elements in the atomic ratio of 1 : 2. As shown in Fig. S2, ESI,† the thickness of the as-prepared large-size PbI_2 nanobelts is measured as 287 ± 94 nm by AFM. Furthermore, the smooth surface of the as-prepared PbI_2

This journal is © The Royal Society of Chemistry 2018

J. Mater. Chem. C, 2018, **6**, 5746–5753 | **5747**
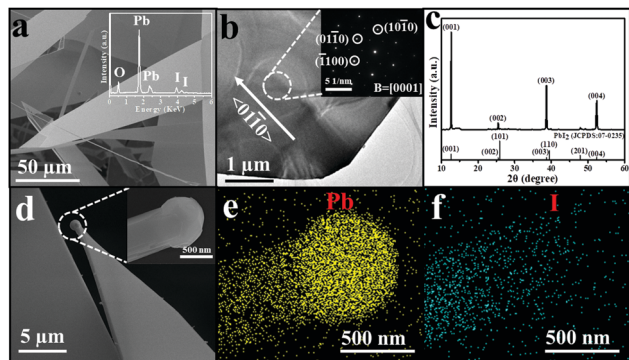
Fig. 1 Morphology, microstructure and composition characterization of the as-prepared large-size PbI$_2$ nanobelts. (a) SEM image of as-prepared PbI$_2$ nanobelts, inset is the corresponding EDS spectrum; (b) TEM image of the as-prepared PbI$_2$ nanobelts, inset is the corresponding SAED image; (c) XRD pattern of the as-prepared PbI$_2$ nanobelts; (d) SEM of the tip section of PbI$_2$ nanobelts, inset is the high-resolution SEM image; (e and f) EDS mapping images of Pb and I of PbI$_2$ nanobelts in figure d inset.

Fig. 2 Effect of source material mass on the nanobelt growth. (a–d) SEM images of the as-prepared PbI$_2$ samples grown with different source material masses of 0.005, 0.01, 0.05 and 0.1 g.

nanobelts is also verified by TEM as shown in Fig. 1b. The SAED pattern in the inset displays the characteristic hexagonal symmetry of diffraction spots with the zone axis of [0001], suggesting that the nanobelts are grown in the $<01\bar{1}0>$ direction with an excellent crystallinity. Based on the XRD pattern of Fig. 1c, the as-prepared PbI$_2$ nanobelts is the hexagonal PbI$_2$ structure (JCPDS: 07-0235) without any other impurity phases, indicating the nanobelts are pure PbI$_2$ crystals.[16,21] This is in line with the SAED result. It is worth pointing out that nanospheres are found at the tip of the as-prepared nanobelts (Fig. 1d), indicating the as-prepared nanobelts follow a VLS growth mechanism.[33,34] This is a common phenomenon of nanoparticles existing on the as-prepared PbI$_2$ nanobelts, as shown in Fig. S3, ESI.† The sizes of the observed nanoparticles are 200–1200 nm. The detailed growth mechanism of this kind of large-size PbI$_2$ nanobelts will be discussed later. As presented in Fig. 1e and f, the EDS elemental mapping of the same nanobelts (inset of Fig. 1d) illustrates the homogeneous distribution of Pb and I atoms along the nanobelt body. In the meanwhile, it is found that the tip mainly contains the Pb atom, whereas the I content drops drastically once passing the tip/nanobelt interface, as shown in Fig. S4, ESI.† In short, all these demonstrate the well-controlled surface morphology, crystallinity and stoichiometry of PbI$_2$ nanobelts achieved with a simple vapor deposition growth technique.

For guiding the controllable growth of large-size 2D nano-materials, the growth mechanism of the as-prepared PbI$_2$ nanobelts is studied in detailed by investigating the mass of source material, growth temperature, and growth time. As shown in SEM images of Fig. 2, one can see that the mass of PbI$_2$ has an important effect on the as-prepared PbI$_2$ morphology. With a low content of 0.005 g PbI$_2$ powder, only nanosheets are found on the substrate. When the mass of PbI$_2$ powder reaches 0.01 g, large-size PbI$_2$ nanobelts with a low density can be observed, possibly caused by the inadequate PbI$_2$ or Pb/I vapor during the nanobelt growth process. Afterwards, as the mass of
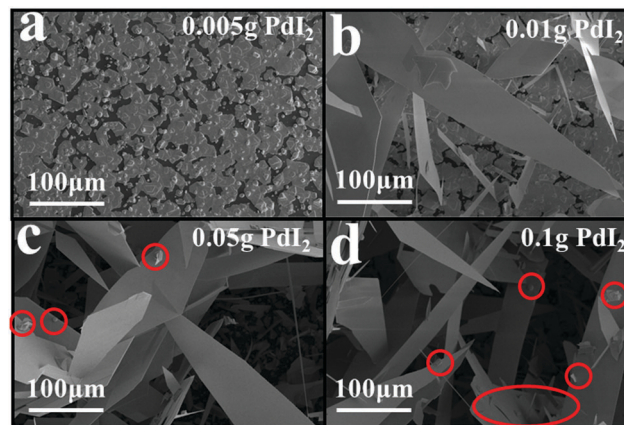
PbI$_2$ powder exceeds the optimal content of 0.015 g, there are small nanosheets grown on the surface of the large-size PbI$_2$ nanobelts, as marked by the red circles in Fig. 2c and d. In a word, as PbI$_2$ has a relatively low melting point of 406 °C,[35] it evaporates easily to form the vapor phase precursors. Therefore, too little source material such as 0.005 g would all be evaporated to form the nanosheets, leading to no successive nanobelt growth. However a higher source mass would provide not only the precursors for nanosheet but also the nanobelt growth. On the other hand, the effect of growth temperature on the controllable growth of PbI$_2$ nanobelts is also studied and the corresponding morphology can be found in Fig. S5, ESI.† Namely, at a low growth temperature of 490 °C, nanosheets dominated the morphology of the as-grown sample. With the increase of growth temperature, the amount of nanobelts increases. However, the width of these as-grown nanobelts is narrow, possibly caused by the inactive PbI$_2$ or Pb/I vapor. Finally, the growth time is also found to be a significant element in the controllable growth of large-size PbI$_2$ nanobelts, as shown in Fig. 3. With a growth time of 1 min, nanosheets together with very short nanobelts are observed on the substrate. When the growth time is prolonged to 5 min, large-size PbI$_2$ nanobelts with a very low density are prepared. Importantly, with a high-resolution SEM image, one can see that the nanobelts are grown
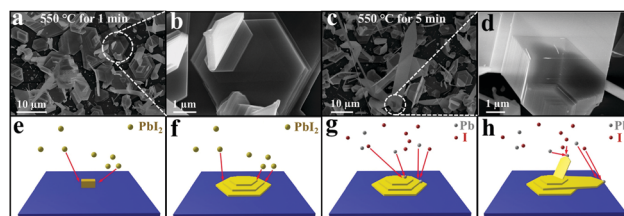
Fig. 3 Possible growth mechanism of the as-prepared large-size PbI$_2$ nanobelts. (a and b) SEM images of PbI$_2$ sample grown at 550 °C for 1 min; (c and d) SEM images of PbI$_2$ sample grown at 550 °C for 5 min; (e–h) schematic illustration of the possible growth process of the as-prepared large-size PbI$_2$ nanobelts.

from the nanosheets randomly. That is, some nanobelts are parallel to the nanosheets and the others are tilted to the nanosheets. The tilt angle can be estimated from XRD pattern in Fig. 1c, where the dominant peaks are related to the c-plane of PbI_2 while only a weak peak is attributed to (201). Therefore, it is plausible that most nanobelts tilt at an angle of $\sim 75°$ which is the one between the (201) and (001) planes. It is worth pointing out that the success in the controlled growth of the large-size PbI_2 nanobelts benefits from the slow heating rate (reach 550 °C in 30 min) of the source material. With a rapid heating rate of the source material (reach 550 °C in 7 min), there are only nanoparticles on the substrate (shown in Fig. S6, ESI†). Anyway, this phenomenon of nanostructures growing from its seed layer is usually found in the growth process of other kinds of nanomaterials.[36–39] In a word, by adopting an optimal growth condition of 0.015 g PbI_2 powder evaporated at 550 °C for 20 min, high-quality and large-size PbI_2 nanobelts with a high density can be prepared on the amorphous SiO_2/Si substrate.

Based on the above discussion, a possible growth mechanism can be proposed here, as shown in Fig. 3e–h. With a slow heating rate of source material, the growth of large-size PbI_2 nanobelts can be divided into two stages. At the first stage, PbI_2 nanosheets grow on the smooth substrate by a PVD process, as reported elsewhere.[19,21,22,26] Namely, at a low growth temperature, the new coming PbI_2 species would get adsorbed on the PbI_2 nuclei as well as on the substrate surface and then migrate to the growth sites. Similar to other types of layered materials, the growth sites of layered PbI_2 nanosheets are always located at the edges as illustrated in Fig. 3e. As a result, the PbI_2 nuclei would then be expanded in the in-plane direction and grow into a large sheet-like structure, as shown in Fig. 3f. With the increase of growth temperature, the evaporated PbI_2 would mostly be decomposed into elemental or molecular Pb and I species. Pb has a higher boiling point of 1749 °C,[40] but a low melting point of 327.4 °C;[40] therefore, it is possible for the Pb species to aggregate into Pb liquid droplets during growth. This result has been verified by the EDS mapping of the as-prepared PbI_2 nanobelts as shown in Fig. 1e and f. Consequently, the PbI_2 nanobelts can then be grown after the catalytic super-saturation of PbI_2 in the Pb liquid droplets via the VLS mechanism. However, with a rapid heating rate of source material, there is not enough time for the PVD growth of the seed layer of PbI_2 nanosheets on the substrate, and thus no nanobelts can be prepared (Fig. S6, ESI†). With a low content of source material, PbI_2 powder would be evaporated off at the first stage of nanosheet growth, resulting in insufficient source vapor for the nanobelt growth. In this case, only the nanosheet can be found on the substrate, as shown in Fig. 2a. With excessive source material, the third PVD/CVD growth process of PbI_2 nanobelts starts at the smooth surface of the as-grown large-size PbI_2 nanobelts. As a result, many irregular nanosheet/nanobelts are observed on the surface of the large-size nanobelts (shown in Fig. 2c and d). With regard to growth temperature, only the PVD growth process occurs at a low growth temperature, and the as-prepared sample shows nanosheets with a few nanobelts (shown in Fig. S5a, ESI†).

However, with the increase of growth temperature, the decomposition of PbI_2 occurs and the contents of Pb and I vapor increase simultaneously, resulting in the successful growth of large-size PbI_2 nanobelts (shown in Fig. S5b–d, ESI†). In short, with a slow heating rate of source material, high-quality, high-density and large-size PbI_2 nanobelts have been prepared successfully from a seed layer of PbI_2 nanosheets by a VLS growth mechanism in a two-step thermal evaporation process.

Raman, UV-vis absorption and PL spectra are carried out to investigate the optical properties of the as-prepared large-size PbI_2 nanobelts. The Raman data of the PbI_2 nanobelts excited by a 532 nm wavelength laser is recorded in Fig. 4a. Three dominant Raman peaks are clearly observed at the locations of 73.8, 97.2, and 112.7 cm^{-1}, corresponding to the E_g, A_{1g}, and A_{2u} Raman vibration modes in the 2H polytype of PbI_2, respectively.[20,26,41,42] Similar with the reported 2D PbI_2 nanostructures, the peak intensity of the as-prepared large-size PbI_2 nanobelts is strong and the corresponding peak's full width at half-maximum (FWHM) is small,[19–22,24,26] indicating a high crystal quality. The UV-vis absorption spectrum is employed to study the bandgap of the as-prepared large-size PbI_2 nanobelts. The experimental values of the bandgap can be obtained through a Kubelka–Munk (K–M) transformation of the UV-visible spectrum: $[F(R)h\nu]^2$, where $F(R)$ is the diffuse reflectance spectrum.[43–45] As shown in Fig. 4b, the calculated bandgap of PbI_2 nanobelts is about 2.36 eV, which coincides well
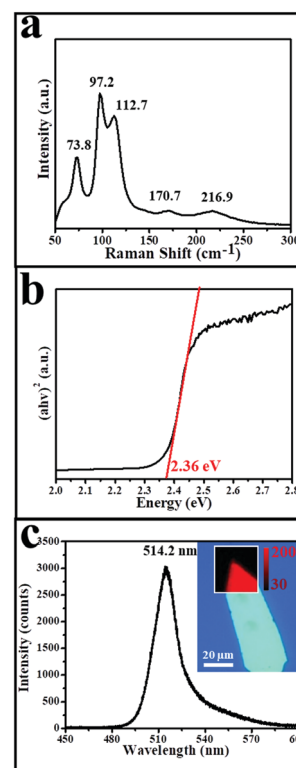
Fig. 4 Optical properties of the as-prepared large-size PbI_2 nanobelts. (a–c) Raman, UV-vis absorption and PL spectra of the as-prepared PbI_2 nanobelts, respectively. Inset of figure c is the 2D PL mapping image at the tip of the as-prepared nanobelt.

This journal is © The Royal Society of Chemistry 2018

J. Mater. Chem. C, 2018, 6, 5746–5753 | 5749

with those of previous reports.[16,19–22,24–27] In addition to the Raman and UV-visible spectra, the room temperature PL spectrum of the as-prepared large-size PbI_2 nanobelts is also obtained, as shown in Fig. 4c. The sharp peak centered at 514 nm (2.41 eV) is in perfect agreement with the bandgap of 2.36 eV determined from the UV-visible spectrum. The strong peak intensity and the narrow FWHM of the PL peak further verify the high crystalline quality of the as-grown large-size PbI_2 nanobelts. This result also can be deduced from the 2D PL mapping image of the as-prepared large-size PbI_2 nanobelts. As depicted in the inset of Fig. 4c, the color contrast of PL mapping is very uniform, indicating the uniform crystallinity of the large-size PbI_2 nanobelts. It is noticeable that there is no 2D PL mapping signal from the Pb nanoparticle, resulting in a black zone at the top of the as-prepared PbI_2 nanobelt, as shown in Fig. S7, ESI.† This phenomenon also can be found in the 2D Raman mapping at a frequency of 97.2 cm^{-1} (PbI_2 domain). However, in Fig. 4c, owing to the low resolution, the black sphere zone of the Pb nanoparticle is so small that it cannot be seen clearly. In short, all these results strongly suggest the potential application of the as-prepared large-size PbI_2 nanobelts with high crystallinity for high-performance optoelectronic devices.

As a direct bandgap semiconductor, besides the understanding of the growth kinetics and mechanisms, it is interesting to assess the optoelectronic properties of the as-prepared large-size PbI_2 nanobelts. In this case, a photodetector is fabricated on the SiO_2/Si substrate by a simple shadow mask process (Si substrate with a 300 nm SiO_2 insulating top layer) and is electrically characterized under illumination. Fig. 5a is the SEM image of the as-fabricated photodetector with a PbI_2 nanobelt area of 879.8 μm^2. Inset is the atomic model of the PbI_2 crystal, displaying PbI_2 as a layered material, which is composed of covalently bonded I–Pb–I repeating units stacked along the c-axis and the van der Waals interlayer interaction. Fig. 5b is the device schematic of the as-fabricated photodetector. Under illumination, the electron–hole will br generated and transformed in the semiconductors. As shown in Fig. S8, ESI,† the current linearly increase with the voltage in current–voltage (I–V) curves, indicating good ohmic contacts between the Au electrodes and PbI_2 nanobelts. At a bias voltage of 5 V, the photocurrents of the as-fabricated photodetector are shown in Fig. 5c under different incident light wavelengths with an intensity of 35 mW cm^{-2}. With an illumination laser wavelength smaller than the bandgap of the as-prepared PbI_2 nanobelts (514 nm), the photocurrent increases with the increase of laser wavelength. On the other hand, no photocurrent can be detected when the illumination laser wavelength is greater than 514 nm. Hence, the 445 nm laser is selected to illuminate the photodetector for better understanding the photosensing behavior of the PbI_2 nanobelts. The dependence of its photocurrent on different light intensities is measured and depicted in Fig. 5d. It is well known that the measured data can be well fitted by equation of $I_p = \alpha\Phi^\beta$, where I_p is the photocurrent, α and β are the fitting parameters, and Φ is the light intensity.[46–51] As a result, the as-fabricated photodetector
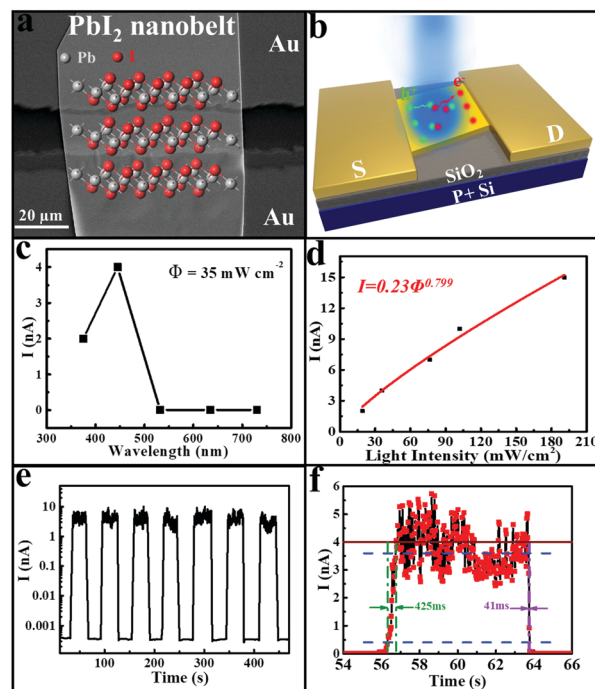
Fig. 5 Photoresponse of the as-prepared large-size PbI_2 nanobelt photodetectors. (a and b) SEM image and device schematic of the as-fabricated photodetector, inset in figure a is the atomic model of the PbI_2 crystal; (c) photocurrent as a function of the incident light wavelength with an intensity of 35 mW cm^{-2}; (d) photocurrent as a function of incident light intensity; (e) the device output current as a function of time under chopped light illumination. The light intensity is 35 mW cm^{-2}; (f) the rise time and decay time constants. The bias voltage for (c–f) is 5 V.

reveals a power dependence of $I_p = 0.23\Phi^{0.799}$ from the fitting of the measured data, depicting the sublinear relationship between the photocurrent and light intensity, which is often observed in layered-material based photoconductors due to the complex processes of electron–hole generation, trapping, and recombination in the semiconductors.[46–48] It is worth pointing out that the value of β is higher than that in the reported 2D nanosheets in the literature,[19,21,22] indicating the high crystallinity of the as-prepared PbI_2 nanobelts. Furthermore, two important figures of merit, responsivity (R) and detectivity (D*), are the key parameters for evaluating the sensitivity of the as-fabricated photodetector. R is defined as the photocurrent generated per unit power of incident light on the effective area of a photodevice, and D* reflects the photodetector's sensitivity. R and D* can be calculated by the following equations: $R = I_p(\Phi S)^{-1}$ and $D* = RS^{1/2}(2eI_d)^{-1/2}$, where I_p is the photocurrent, Φ is the light intensity, S is the active area of the photodetector, e is the absolute value of the charge of an electron, and I_d is the dark current.[52–55] For the large-size PbI_2 nanobelt based photodetector, the maximum R and the corresponding D* are calculated to be about 13 mA W^{-1}, and 3.048 × 10^{10} Jones across the entire measured range, respectively, comparable to the graphene photodetectors (0.5–6.1 mA W^{-1})[56,57] and the single-crystal CdTe nanosheets (0.6 mA W^{-1}).[58] The repeatability and response speed are another two essential

5750 | J. Mater. Chem. C, 2018, 6, 5746–5753

This journal is © The Royal Society of Chemistry 2018

Table 1 Comparison of various figures of merit of different representative 2D layered PbI_2 based photodetectors

Morphology	Light (nm)	Bias (V)	Dark current (pA)	On/off ratio	Rise time (ms)	Decay time (ms)	Ref.
Nanobelt	445	5	4	10^3	425	41	This work
Single crystal	440	15	1380	10^2		0.354	16
Monolayer nanosheet	450	5		10	18	22	22
Nanosheet	405	5	5.1	42	86	150	21
Nanosheet	450	5	10	10^3	18	22	19
Nanosheet	405	1	5	2000			24
Single crystal	450	10	560	10^4	0.323	0.52	25
Flake	470	5	0.14	900	13.5	20	26
Nanosheet	450	1.9	0.01	10^2	0.055	0.11	20

parameters for the performance assessment of photodetectors. The repeatability can be appraised by measuring the photocurrent as a function of time (*i.e.*, *I*–*t* curves) under chopped illumination as shown in Fig. 5e. It is obvious that the device ON- and OFF-state can be effectively modulated by the chopped illumination with a good repeatability and an impressive ON/OFF current ratio of 10^3–10^4. It is worth pointing out that the photodetector also has a low dark current of 4 pA when the laser is in the "OFF" state. The low value of the dark current indicates a low noise and a high sensitivity, which are vital for practical electric-devices. In addition, a high-resolution *I*–*t* curve is then utilized to study the response speed of the photodetector. Usually, the times needed for the current to increase from 10% to 90% of the peak value and *vice versa* are defined as the rise time and decay time constants, respectively.[59,60] Based on the measurement presented in Fig. 5f, the rise and decay time constants can be identified as 425 and 41 ms accordingly, implying the high quality of the as-prepared large-size PbI_2 nanobelts. Regardless, all these obtained performance indicators of nanobelt detectors are highly comparable to those of the state-of-the-art PbI_2 as reported in the recent literature (Table 1), illustrating the impressive performance and promising prospects of our larger-size PbI_2 nanobelts for highly-efficient photodetection. It is worth pointing out that the rise and decay times are related to the recombination of nonequilibrium photo-generated carriers. The combination processes can be affected by many factors, such as trap density, trap energy level in the forbidden gap, surface states, adsorbed molecules, *etc.* These factors are not only related to the quality of the photosensing materials, but also related to the device fabrication processes. Although our PbI_2 nanobelts have high quality, the device fabrication processes can also degrade the performance of the response speed. Further optimizations of device fabrication process are needed in the future.

followed by the CVD growth of large-size PbI_2 nanobelts at a higher growth temperature by using the as-grown PbI_2 nanosheets as a seed layer. The results of SAED and PL measurements confirm the highly uniform, high-quality crystallinity of the as-prepared large-size PbI_2 nanobelts. The as-prepared PbI_2 nanobelt based photodetector exhibits a low dark current of 4 pA, an impressive ON/OFF current ratio of 10^3–10^4, a photoresponsivity of 13 mA W^{-1}, and a fast response with rise and decay time constants of 425 and 41 ms, respectively, with a large area PbI_2 nanobelt of 879.8 μm^2. All the discussed parameters reveal the technological potency of these large-size PbI_2 nanobelts for next-generation high-performance optoelectronics.

Authors contribution

Zai-xing Yang and Ning Han conceived and designed the research. Mingming Han grew the nanobelts. Jiamin Sun implemented the XRD measurement and analysis. Mingming Han and Luozhen Bian performed the SEM, PL and Raman measurement and analysis. Jiamin Sun and Luozhen Bian measured UV-vis absorption and analysis. Mingming Han, Jiamin Sun and Luozhen Bian carried out the device fabrication. Zhou Wang contributed to the photodetection test. Lei Zhang performed the TEM measurement. Yanxue Yin, Zhaofeng Gao and Fulin Li contributed to the data analysis of TEM and photodetection. Zai-xing Yang, Ning Han, Qian Xin, Longbin He and Aimin Song prepared the manuscript with help from all of the other co-authors.

Conflicts of interest

There are no conflicts to declare.

Acknowledgements

Conclusions

In conclusion, the large-scale synthesis of large-size PbI_2 nanobelts is successfully demonstrated by manipulating the source material mass, growth temperature, and growth time on an amorphous Si/SiO_2 substrate in a two-step vapor deposition process. With a slow heating rate of the growth temperature, the PVD growth process of PbI_2 nanosheets occurs firstly,

References

1 M. J. Allen, V. C. Tung and R. B. Kaner, *Chem. Rev.*, 2010, **110**, 132–145.

2 Q. H. Wang, K. Kalantar-Zadeh, A. Kis, J. N. Coleman and M. S. Strano, *Nat. Nanotechnol.*, 2012, **7**, 699–712.

3 G. R. Bhimanapati, Z. Lin, V. Meunier, Y. Jung, J. Cha, S. Das, D. Xiao, Y. Son, M. S. Strano, V. R. Cooper, L. Liang, S. G. Louie, E. Ringe, W. Zhou, S. S. Kim, R. R. Naik, B. G. Sumpter, H. Terrones, F. Xia, Y. Wang, J. Zhu, D. Akinwande, N. Alem, J. A. Schuller, R. E. Schaak, M. Terrones and J. A. Robinson, *ACS Nano*, 2015, **9**, 11509–11539.

4 K. F. Mak and J. Shan, *Nat. Photonics*, 2016, **10**, 216–226.

5 K. S. Novoselov, A. Mishchenko, A. Carvalho and A. H. Castro Neto, *Science*, 2016, **353**, 9439.

6 Q. Guo, A. Pospischil, M. Bhuiyan, H. Jiang, H. Tian, D. Farmer, B. Deng, C. Li, S.-J. Han, H. Wang, Q. Xia, T.-P. Ma, T. Mueller and F. Xia, *Nano Lett.*, 2016, **16**, 4648–4655.

7 J. S. Ponraj, Z.-Q. Xu, S. C. Dhanabalan, H. Mu, Y. Wang, J. Yuan, P. Li, S. Thakur, M. Ashrafi, K. McCoubrey, Y. Zhang, S. Li, H. Zhang and Q. Bao, *Nanotechnology*, 2016, **27**, 462001.

8 M. Pumera and Z. Sofer, *Adv. Mater.*, 2017, **29**, 1605299.

9 Y.-R. Chang, P.-H. Ho, C.-Y. Wen, T.-P. Chen, S.-S. Li, J.-Y. Wang, M.-K. Li, C.-A. Tsai, R. Sankar, W.-H. Wang, P.-W. Chiu, F.-C. Chou and C.-W. Chen, *ACS Photonics*, 2017, **4**, 2930–2936.

10 M. Sun, D. Xie, Y. Sun, W. Li and T. Ren, *Nanotechnology*, 2018, **29**, 015203.

11 Z. Fang, Z. Liu, Y. Wang, P. M. Ajayan, P. Nordlander and N. J. Halas, *Nano Lett.*, 2012, **12**, 3808–3813.

12 Z. Fang, Y. Wang, Z. Liu, A. Schlather, P. M. Ajayan, F. H. Koppens, P. Nordlander and N. J. Halas, *ACS Nano*, 2012, **6**, 10222–10228.

13 J. Song, L. Xu, J. Li, J. Xue, Y. Dong, X. Li and H. Zeng, *Adv. Mater.*, 2016, **28**, 4861–4869.

14 H. Deng, X. Yang, D. Dong, B. Li, D. Yang, S. Yuan, K. Qiao, Y.-B. Cheng, J. Tang and H. Song, *Nano Lett.*, 2015, **15**, 7963–7969.

15 G. Wang, D. Li, H.-C. Cheng, Y. Li, C.-Y. Chen, A. Yin, Z. Zhao, Z. Lin, H. Wu, Q. He, M. Ding, Y. Liu, Y. Huang and X. Duan, *Sci. Adv.*, 2015, **1**, 1500613.

16 J. Zhang, T. Song, Z. Zhang, K. Ding, F. Huang and B. Sun, *J. Mater. Chem. C*, 2015, **3**, 4402–4406.

17 S. Yakunin, D. N. Dirin, Y. Shynkarenko, V. Morad, I. Cherniukh, O. Nazarenko, D. Kreil, T. Nauser and M. V. Kovalenko, *Nat. Photonics*, 2016, **10**, 585–589.

18 H.-C. Cheng, G. Wang, D. Li, Q. He, A. Yin, Y. Liu, H. Wu, M. Ding, Y. Huang and X. Duan, *Nano Lett.*, 2016, **16**, 367–373.

19 M. Zhong, L. Huang, H.-X. Deng, X. Wang, B. Li, Z. Wei and J. Li, *J. Mater. Chem. C*, 2016, **4**, 6492.

20 W. Zheng, Z. Zhang, R. Lin, K. Xu, J. He and F. Huang, *Adv. Electron. Mater.*, 2016, **2**, 1600291.

21 C. Lan, R. Dong, Z. Zhou, L. Shu, D. Li, S. Yip and J. C. Ho, *Adv. Mater.*, 2017, **29**, 1702759.

22 M. Zhong, S. Zhang, L. Huang, J. You, Z. Wei, X. Liu and J. Li, *Nanoscale*, 2017, **9**, 3736–3741.

23 J. K. Meyers, S. Kim, D. J. Hill, E. E. M. Cating, L. J. Williams, A. S. Kumbhar, J. R. McBride, J. M. Papanikolas and J. F. Cahoon, *Nano Lett.*, 2017, **17**, 7561.

24 R. Frisenda, J. O. Island, J. L. Lado, E. Giovanelli, P. Gant, P. Nagler, S. Bange, J. M. Lupton, C. Schller, A. J. Molina-Mendoza, L. Aballe, M. Foerster, T. Korn, M. A. Nino, D. P. de Lara, E. M. Perez, J. Fernandez-Rossier and A. Castellanos-Gomez, *Nanotechnology*, 2017, **28**, 455703.

25 Q. Wei, B. Shen, Y. Chen, B. Xu, Y. Xia, J. Yin and Z. Liu, *Mater. Lett.*, 2017, **193**, 101–104.

26 Y. Wang, L. Gan, J. Chen, R. Yang and T. Zhai, *Sci. Bull.*, 2017, **62**, 1654–1662.

27 J. Liu, Z. Liang, B. Xu, H. Xiang, Y. Xia, J. Yin and Z. Liu, *RSC Adv.*, 2016, **6**, 59445–59449.

28 V. K. Agrawal, G. K. Chadha and G. C. Trigunay, *Acta Crystallogr., Sect. A: Cryst. Phys., Diffr., Theor. Gen. Crystallogr.*, 1970, **A26**, 140.

29 M. R. Tubbs, *Phys. Status Solidi B*, 1972, **49**, 11.

30 Z.-X. Yang, W. Zhong, P. Zhang, M.-H. Xu, C.-T. Au and Y.-W. Du, *CrystEngComm*, 2012, **14**, 585–589.

31 Z.-x. Yang, N. Han, F. Wang, H.-Y. Cheung, X. Shi, S. Yip, T. Hung, M. H. Lee, C.-Y. Wong and J. C. Ho, *Nanoscale*, 2013, **5**, 9671–9676.

32 Z.-X. Yang, W. Zhong, C.-T. Au and Y.-W. Du, *Chin. Phys. B*, 2013, **22**, 108101.

33 R. S. Wagner and W. C. Ellis, *Appl. Phys. Lett.*, 1964, **4**, 89.

34 J. Westwater, D. P. Gosain, S. Tomiya, S. Usui and H. Ruda, *J. Vac. Sci. Technol., B*, 1997, **15**, 554–557.

35 R. J. M. Konings, E. H. P. Cordfunke and R. R. Vanderlaan, *J. Alloys Compd.*, 1995, **230**, 85–88.

36 L. E. Greene, M. Law, D. H. Tan, M. Montano, J. Goldberger, G. Somorjai and P. D. Yang, *Nano Lett.*, 2005, **5**, 1231–1236.

37 M. Law, L. E. Greene, J. C. Johnson, R. Saykally and P. D. Yang, *Nat. Mater.*, 2005, **4**, 455–459.

38 Z. X. Yang, W. Zhong, C. T. Au, X. Du, H. A. Song, X. S. Qi, X. J. Ye, M. H. Xu and Y. W. Du, *J. Phys. Chem. C*, 2009, **113**, 21269–21273.

39 S. Xu and Z. L. Wang, *Nano Res.*, 2011, **4**, 1013–1098.

40 D. R. Lide, *CRC Handbook of Chemistry and Physics*, 85th edn, CRC Press, 2004.

41 W. M. Sears, M. L. Klein and J. A. Morrison, *Phys. Rev. B: Condens. Matter Mater. Phys.*, 1979, **19**, 2305–2313.

42 N. Preda, L. Mihut, M. Baibarac, I. Baltog and S. Lefrant, *J. Phys.: Condens. Matter*, 2006, **18**, 8899–8912.

43 R. R. Anderson and J. A. Parrish, *J. Invest. Dermatol.*, 1981, **77**, 13–19.

44 A. F. da Silva, N. Veissid, C. Y. An, I. Pepe, N. B. de Oliveira and A. V. B. da Silva, *Appl. Phys. Lett.*, 1996, **69**, 1930–1932.

5752 | *J. Mater. Chem. C*, 2018, **6**, 5746–5753

This journal is © The Royal Society of Chemistry 2018

45 X. H. Zhu, Z. R. Wei, Y. R. Jin and A. P. Xiang, *Cryst. Res. Technol.*, 2007, **42**, 456–459.

46 F. Binet, J. Y. Duboz, E. Rosencher, F. Scholz and V. Harle, *Appl. Phys. Lett.*, 1996, **69**, 1202–1204.

47 C. Soci, A. Zhang, B. Xiang, S. A. Dayeh, D. P. R. Aplin, J. Park, X. Y. Bao, Y. H. Lo and D. Wang, *Nano Lett.*, 2007, **7**, 1003–1009.

48 O. Lopez-Sanchez, D. Lembke, M. Kayci, A. Radenovic and A. Kis, *Nat. Nanotechnol.*, 2013, **8**, 497–501.

49 X. Wang, P. Wang, J. Wang, W. Hu, X. Zhou, N. Guo, H. Huang, S. Sun, H. Shen, T. Lin, M. Tang, L. Liao, A. Jiang, J. Sun, X. Meng, X. Chen, W. Lu and J. Chu, *Adv. Mater.*, 2015, **27**, 6575.

50 C. Y. Lan, C. Li, S. Wang, T. Y. He, Z. F. Zhou, D. P. Wei, H. Y. Guo, H. Yang and Y. Liu, *J. Mater. Chem. C*, 2017, **5**, 1494–1500.

51 B. Du, W. Yang, Q. Jiang, H. Shan, D. Luo, B. Li, W. Tang, F. Lin, B. Shen, Q. Gong, X. Zhu, R. Zhu and Z. Fang, *Adv. Opt. Mater.*, 2018, **6**, 1701271.

52 G. Konstantatos and E. H. Sargent, *Nat. Nanotechnol.*, 2010, **5**, 391–400.

53 J. Michel, J. Liu and L. C. Kimerling, *Nat. Photonics*, 2010, **4**, 527–534.

54 L. Rigutti, M. Tchernycheva, A. D. L. Bugallo, G. Jacopin, F. H. Julien, L. F. Zagonel, K. March, O. Stephan, M. Kociak and R. Songmuang, *Nano Lett.*, 2010, **10**, 2939–2943.

55 L. Peng, L. Hu and X. Fang, *Adv. Mater.*, 2013, **25**, 5321–5328.

56 F. Xia, T. Mueller, Y.-m. Lin, A. Valdes-Garcia and P. Avouris, *Nat. Nanotechnol.*, 2009, **4**, 839–843.

57 M. Freitag, T. Low, F. Xia and P. Avouris, *Nat. Photonics*, 2013, **7**, 53–59.

58 R. Cheng, Y. Wen, L. Yin, F. Wang, F. Wang, K. Liu, T. A. Shifa, J. Li, C. Jiang, Z. Wang and J. He, *Adv. Mater.*, 2017, **29**, 1703122.

59 M. Buscema, D. J. Groenendijk, S. I. Blanter, G. A. Steele, H. S. J. van der Zant and A. Castellanos-Gomez, *Nano Lett.*, 2014, **14**, 3347–3352.

60 R. Saran and R. J. Curry, *Nat. Photonics*, 2016, **10**, 81–92.